

# Nuclear fragmentation/dispersion modeling and simulation of hazardous near-Earth objects



Brian Kaplinger<sup>a,\*</sup>, Bong Wie<sup>a</sup>, David Dearborn<sup>b</sup>

<sup>a</sup> Asteroid Deflection Research Center, Iowa State University, 2271 Howe Hall, Ames, IA 50011, United States

<sup>b</sup> Lawrence Livermore National Laboratory, 7000 East Avenue, Livermore, CA 94550, United States

## ARTICLE INFO

### Article history:

Received 1 March 2012

Received in revised form

20 August 2012

Accepted 1 October 2012

Available online 17 November 2012

### Keywords:

Near-Earth objects

Nuclear fragmentation and dispersion

Subsurface explosion

Penetrating contact burst

GPU

## ABSTRACT

This paper presents the development of simulation tools designed to be implemented as part of the mission design procedure for nuclear fragmentation and dispersion of a near-Earth object (NEO). A description of the methods used will be presented, followed by a discussion of the advanced GPU (Graphics Processing Unit) computing technology applied to accelerate computation. Preliminary results of a fragmented NEO dispersion scenario emphasize global parameter search methods for use in engineering mission analysis. A model of the NEO fragmentation process is presented for a subsurface nuclear explosion and penetrating contact burst. We conduct Monte Carlo simulation to establish a mean response of the target NEO to the fragmentation process. Resulting coherent masses are propagated through a model of solar system dynamics until the predetermined date of impact. On some orbits, the impacting mass can be reduced to lower than 0.1% of the NEO mass.

© 2012 IAA. Published by Elsevier Ltd. All rights reserved.

## 1. Introduction

Asteroids have impacted the Earth in the past and threaten to do so in the future. While the most likely near-term threat is that of a low-altitude airburst, the expected energy of an event such as Tunguska would be devastating in a highly populated area. Additionally, though the population of catastrophic impactors has been well surveyed, it is estimated that thousands of bodies over 140 m in diameter remain undiscovered [1]. Many methods have been suggested for the mitigation of this threat, but most require substantial lead time in order to be effective. A study by the United States National Research Council suggests that nuclear explosive devices may be the only option for late warning cases [2]. Sanchez et al. [3], provide an analytical framework discussing how fragmentation at low energy can be an undesirable effect,

despite the dispersion along the orbit of the resulting fragments. Previous simulations show that disruption at higher energies may substantially reduce the amount of mass remaining on impact trajectories. This method could be available with as little as 10 days of lead time between intercept and the predicted impact date for an orbit like that of the asteroid Apophis [4].

A major bottleneck in determining appropriate mitigation methods for near-Earth objects (NEOs) has been a lack of experimental data on the efficacy of each approach, forcing a reliance on simulations to determine mission effectiveness. As we move from the concept stage into true mission planning for effective NEO threat mitigation, we must depart from simulation of a few sample cases and instead use actual mission parameters to integrate modeling and simulation into the mission design cycle. This paper presents the development of simulation tools designed to be implemented as part of the mission design procedure for nuclear fragmentation and dispersion of an NEO. A description of the methods used will be presented, followed by a discussion of the

\* Corresponding author. Tel.: + 1 515 294 3124.

E-mail address: [bdkaplin@iastate.edu](mailto:bdkaplin@iastate.edu) (B. Kaplinger).

advanced GPU (Graphics Processing Unit) computing technology applied to accelerate computation. Preliminary results of a fragmented NEO dispersion scenario are discussed, emphasizing global parameter search methods for use in engineering mission analysis. A model of the NEO fragmentation process is presented for a subsurface nuclear explosion and penetrating contact burst. A Smoothed Particle Hydrodynamics (SPH) code is used to compare the results to past studies of nuclear shock propagation in brittle material and current research in hypervelocity impacts. This approach is contrasted to Arbitrary Lagrangian–Eulerian (ALE) codes in current use at the Lawrence Livermore National Laboratory for asteroid fragmentation simulation.

We assume an isotropic Weibull distribution of implicit flaws in the NEO material and conduct Monte Carlo simulation to establish a mean response of the target NEO to the fragmentation process. Resulting coherent masses are propagated through a model of solar system dynamics until the predetermined date of impact. Masses remaining on impact trajectories undergo a simulation of reentry into Earth's atmosphere, resulting in final tallies of mass missing the Earth, fragments on capture trajectories, airburst events, and impacts of reduced-mass fragments. Past results show that, on some orbits, the impacting mass can be reduced to lower than 0.1% of the NEO mass. The present paper addresses a modular framework for NEO structures to provide guidelines for mission design analysis.

Historically, simulations have been limited to a few large test cases to demonstrate the viability of planetary defense options. This paper addresses the use of GPU computation, a new direction in high-performance computing (HPC), to achieve up to 150x faster computation in a workstation form factor [4]. A dedicated compute server has been shown to be over 400x as fast as CPU implementation, and these are far cheaper than their HPC cluster and supercomputer counterparts [5,6]. This has allowed for a revolution in computing on a budget, allowing hundreds of complex simulations to be tested. While new HPC technology is shown to solve old problems faster, this paper also addresses the identification of new problems that were previously intractable without the use of a supercomputer. Specific performance and results from several GPU compute configurations will be presented. Disruption of an NEO (i.e. fragmentation and dispersion) has been shown to be a viable option using current technology for worst-case mission scenarios with a short warning time. An extended characterization of disruption scenarios is discussed, and an effort is made to determine needed technological requirements for general nuclear disruption effectiveness. Use of improvements to fragmentation modeling, reentry modeling, and orbital dispersion modeling [4] are presented.

## 2. Fragmentation model

This section presents the asteroid models being considered. While spherical bodies have been assumed for convenience, it is important to note that any valid three-dimensional geometry can be processed by the current

simulation framework. The resulting fragmented system is intended to be statistical in nature, so a Direct Simulation Monte Carlo (DSMC) approach is taken to identify expected system characteristics. This is done by varying the Weibull exponent for each run, with a uniform distribution across the range indicated.

### 2.1. Previous ALE static results

In previous work [5,7,8], a 270-m diameter Apophis-like asteroid model was developed with a total mass of 2.058E10 kg. This example was run using the CALE code (C-language-based Arbitrary Lagrangian–Eulerian), a two-dimensional hydrodynamic code developed at Lawrence Livermore National Laboratory. This model was comprised of two main parts (inhomogeneous), as shown in Fig. 1. The core of the asteroid was solid granite with a density of 2630.0 kg/m<sup>3</sup>, while the outer mantle was a “rubble pile” of density 1910 kg/m<sup>3</sup>. This results in a bulk asteroid density of 1990 kg/m<sup>3</sup>, similar to that measured for the asteroid Itokawa. Linear strength modeling was used in the core, with a yield strength of 14.6 MPa and a shear modulus of 35 MPa. A static (non-moving) nuclear explosive is detonated in a 5 meter subsurface cavity, resulting in an energy source equivalent to 300 kt [7]. The resulting system shown in Fig. 2 has a clear direction of maximum momentum, with radially distributed fragments dispersing from the center of mass with velocities far in excess of the local escape velocity. The orbital dynamics of this system for an orbit similar to that of Apophis has been extensively studied [4,5,8], and this deflection could result in as little as 0.1% of the asteroid mass remaining on impacting trajectories.

### 2.2. Smoothed Particle Hydrodynamics model

For the purposes of the present simulation study, a meshless hydrodynamics model was desired. This approach would eliminate the need for storing and updating a grid, simplify calculations for large deformations, and allow for contiguous memory access to local field properties. The SPH formulation [9,10] was chosen to satisfy the first two goals, while the latter will be discussed with regards to the GPU implementation.

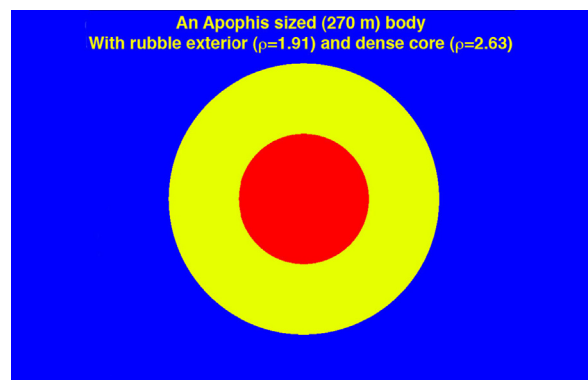


Fig. 1. An internal composition model of a 270-m NEO [4].

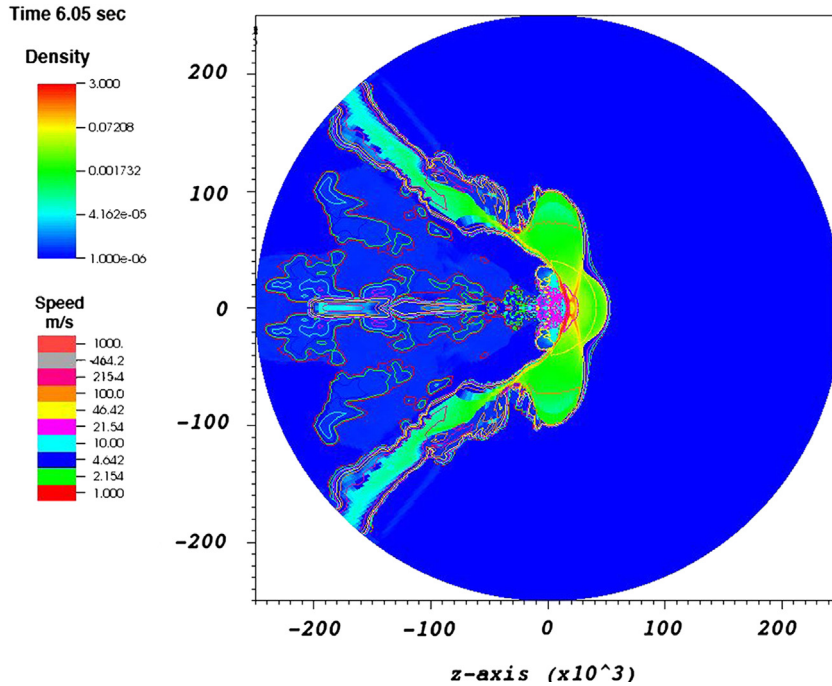


Fig. 2. Fragment distribution of static ALE results [4].

The core idea of SPH is to approximate a field property  $f(x)$  using a mollifier  $W$  (also known as an approximate identity) with compact support

$$\langle f(x) \rangle = \int_{\Omega} f(s)W(x-s) ds,$$

$$W \in C_0^1(\mathbb{R}^n), \Omega = \text{supp}(W) \quad (1)$$

where the brackets indicate the SPH approximation [10], allowing the field variables to be computed as a sum over the nearest neighbor particles representing the flow. In the present formulation,  $W$  is taken as the cubic spline kernel [9,10], with a variable isotropic domain of support with radius  $h$ . Changing  $h$  in space and time allows for the simulation to respond to changes in flow conditions with a change in local resolution [9,10]. A mass  $m$  is assigned to each particle representative in the model, as well as initial position and velocity components ( $x^\beta$  and  $v^\beta$ ) in each  $\beta$  direction. Material properties such as density,  $\rho$ , and specific energy,  $e$ , complete the state description. Similar to the above integral relationship, derivatives and integrals of field functions can be approximated, resulting in the following set of [9–11] involving the kernel derivative (a scalar valued function of vector position  $\mathbf{x}$ ):

$$\frac{Dx_i^\alpha}{Dt} = v_i^\alpha$$

$$\frac{D\rho_i}{Dt} = \sum_{j=1}^N m_j (v_i^\beta - v_j^\beta) \frac{\partial W}{\partial x^\beta}(\mathbf{x}_j - \mathbf{x}_i)$$

$$\frac{Dv_i^\alpha}{Dt} = - \sum_{j=1}^N m_j \left( \frac{\sigma_i^{\alpha\beta}}{\rho_i^2} + \frac{\sigma_j^{\alpha\beta}}{\rho_j^2} + \Pi_{ij} \right) \frac{\partial W}{\partial x^\beta}(\mathbf{x}_j - \mathbf{x}_i) + F_i^\alpha$$

$$\begin{aligned} \frac{De_i}{Dt} = & \frac{1}{2} \sum_{j=1}^N m_j \left( \frac{P_i}{\rho_i^2} + \frac{P_j}{\rho_j^2} + \Pi_{ij} \right) (v_i^\beta - v_j^\beta) \frac{\partial W}{\partial x^\beta}(\mathbf{x}_j - \mathbf{x}_i) \\ & + \frac{1}{\rho_i} S_i^{\alpha\beta} \epsilon_i^{\alpha\beta} + H_i \end{aligned} \quad (2)$$

where repeated indices in a product indicate implied summation over all possible values,  $\sigma^{\alpha\beta}$  is the stress tensor,  $P$  is the pressure,  $S^{\alpha\beta}$  is the deviatoric (traceless) stress tensor,  $\epsilon^{\alpha\beta}$  is the local strain rate tensor,  $F$  represents external forces, and  $H$  represents energy sources.  $\Pi$  represents the Monaghan numerical viscosity [10,12] used to resolve shocks, accommodate heating along the shock, and resist unphysical material penetration. The material strength model for the core uses an elastic-perfectly plastic description of strength [9–11], where the hydrodynamic stress is determined as

$$\sigma_i^{\alpha\beta} = -P_i \delta^{\alpha\beta} + (1-\eta) S_i^{\alpha\beta}, \quad \eta \in [0,1] \quad (3)$$

where  $\eta$  is a material damage indicator, to be discussed later. It should be noted that fully damaged material ( $\eta = 1$ ) is relieved of all stress due to deformation and behaves as a cohesionless fluid [11,13]. In this elastic-plastic model, the components of the deviatoric stress tensor  $S^{\alpha\beta}$  evolve using the following equation based on Hooke's law [9,14]:

$$\frac{DS_i^{\alpha\beta}}{Dt} = 2\mu \left( \epsilon_i^{\alpha\beta} - \frac{1}{3} \delta^{\alpha\beta} \epsilon_i^{\gamma\gamma} \right) + S_i^{\alpha\gamma} R_i^{\beta\gamma} + R_i^{\alpha\gamma} S_i^{\gamma\beta} \quad (4)$$

where  $R^{\alpha\beta}$  is the local rotation rate tensor,  $\mu$  is the shear modulus, and the SPH approximation for these terms is

given by

$$\epsilon_i^{\alpha\beta} = \frac{1}{2} \sum_{j=1}^N \frac{m_j}{\rho_j} \left[ (v_j^\alpha - v_i^\alpha) \frac{\partial W}{\partial x^\beta} (\mathbf{x}_j - \mathbf{x}_i) + (v_j^\beta - v_i^\beta) \frac{\partial W}{\partial x^\alpha} (\mathbf{x}_j - \mathbf{x}_i) \right]$$

$$R_i^{\alpha\beta} = \frac{1}{2} \sum_{j=1}^N \frac{m_j}{\rho_j} \left[ (v_j^\alpha - v_i^\alpha) \frac{\partial W}{\partial x^\beta} (\mathbf{x}_j - \mathbf{x}_i) - (v_j^\beta - v_i^\beta) \frac{\partial W}{\partial x^\alpha} (\mathbf{x}_j - \mathbf{x}_i) \right]$$

To complete this system, we use the following equations governing the change of support radius  $h$  [9,10], and the fracture damage ratio  $\eta$  [11]. The latter is limited in accordance with the number of material flaws activated in the structure, as described in the next section:

$$\frac{Dh_i}{Dt} = -\frac{1}{n} \frac{h_i D\rho_i}{\rho_i Dt}, \quad \frac{D}{Dt} \eta^{1/3} = \frac{c_g}{r_s} \quad (5)$$

where  $c_g$  is the crack growth rate, here assumed to be 0.4 times the local sound speed [11], and  $r_s$  is the radius of the subvolume subject to tensile strain. In the present model, the latter term is estimated by interpolation based on the strain rate tensor of neighbor particles. An equation of state remains to complete the mechanical system. We use the Tillotson equation of state [15] in the solid asteroid core and in the Al penetrator used to deliver the explosive. This is modified to include a porosity of 0.1, and an irreversible crush strength of 12 MPa, for the outer “rubble pile” layer [13,16]. The parameters used are shown in Table 1.

### 2.3. Implicit flaw assignment

We assume a power law distribution for number of implicit flaws in a volume of material with respect to local tensile strain (a Weibull distribution), and assign flaws with specific activation thresholds to each SPH particle [11]. The behavior of the core material under high stress is governed by the activation of these implicit flaws. These flaws are seeded in the representation particles using a coefficient of around 4.2E23 and an exponent between 6.2 and 9.5. Using a range of distribution exponents and strength properties allows us to examine the behavior of the core material with varying brittleness and material cohesion. The maximum damage allowed to accumulate in a volume is

$$\eta_i^{\max} = \left( \frac{n_i}{n_i^{\text{tot}}} \right)^{1/3}, \quad \epsilon_i = \frac{\sigma_i^t}{(1-\eta_i)E} \quad (6)$$

**Table 1**  
Parameters for Tillotson equation of state in core material.

| Parameter  | Numerical value | Units |
|------------|-----------------|-------|
| $a_t$      | 0.5             |       |
| $b_t$      | 1.5             |       |
| $A_t$      | 7.1E10          | Pa    |
| $B_t$      | 7.5E10          | Pa    |
| $\alpha_t$ | 5               |       |
| $\beta_t$  | 5               |       |
| $E_0$      | 4.87E8          | J/kg  |
| $E_{iv}$   | 4.72E6          | J/kg  |
| $E_{cv}$   | 1.82E7          | J/kg  |

where  $n$  is the number of active flaws ( $\epsilon > \epsilon^{\text{act}}$ ) and  $n^{\text{tot}}$  is the total number of flaws assigned to a particle, which can vary widely, but is always at least one. Eq. (6) also gives the relationship for the local scalar strain, as a function of the maximum tensile stress  $\sigma^t$ , the local damage, and the Young’s modulus  $E$ .

### 2.4. Explosive penetrator

The present models use a starting resolution of 0.1 m for two target asteroids with diameters of 270 m and 54 m, resulting in 1.4 million and 233,000 fragments, respectively. A penetrator impacts the asteroid at a velocity of 6.1 km/s, and explode on contact, sourcing 300 kt and 60 kt into the model, respectively. The penetrator in this example is an Al sphere, with the inner 1/3 (by radius) considered to be the explosive system. Thus, the energy is deposited in the inner region of the Al penetrator when the impact shock reaches this boundary (about 1 ms). Since the convection time is much larger than the representative time of the hydrodynamics, thermal energy transfer in addition to the SPH energy balance described was not addressed for this example. In addition, radiative heat transfer of the resulting explosive gas and asteroid material is not currently implemented.

While the fragmentation model results in different results each time, we can average multiple runs to achieve a mean distribution that is representative of the physical situation. This simulation is not intended to be a prediction, but rather a way to determine general system behavior to identify particularly effective methods for disruption. The present SPH model is extremely fast, and is a good option for describing a fragmented asteroid system due to an explosive penetrator.

## 3. Orbital dispersion model

This section describes the orbital model used to propagate fragment trajectories. A 2D SPH implementation has been used for the current work, which estimates the behavior of a planar slice of the problem. The fragments are then given a random azimuth for the orbital calculations. The nominal orbit chosen is close to that of Apophis post-2029, with slight alterations made to ensure impact in our model on April 13, 2036. The parameters for this orbit are given in Table 2.

The debris cloud is given global coordinates in a Local-Vertical-Local-Horizontal (LVLH) reference frame about

**Table 2**  
Orbital parameters for 15-day impact trajectory.

| Orbital parameter            | Value                        |
|------------------------------|------------------------------|
| Semimajor axis               | 1.1082428 AU                 |
| Eccentricity                 | 0.189928428                  |
| Inclination                  | 2.18995362 deg               |
| Longitude of right ascension | 203.18642266 deg             |
| Argument of perihelion       | 69.929774 deg                |
| Initial mean anomaly         | 296.74684241 deg             |
| Epoch                        | 64,781 MJD                   |
| Miss distance on target date | 4.738466849E-011 Earth radii |

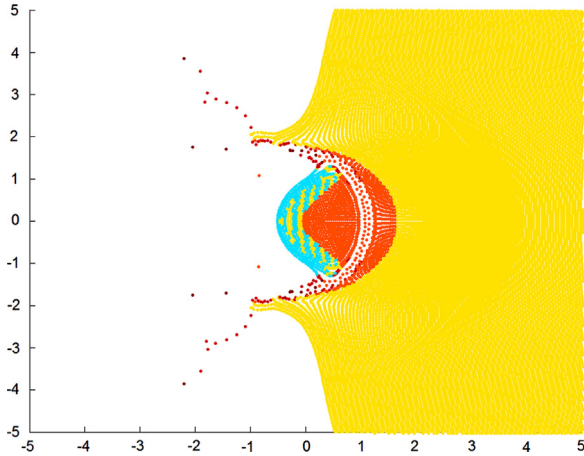


Fig. 3. 270-m asteroid penetration at 1.2 ms.

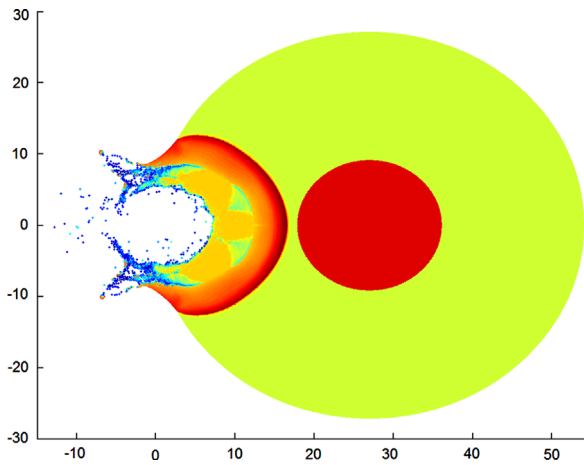


Fig. 4. Expanding shock wave through rubble at 2.3 ms.

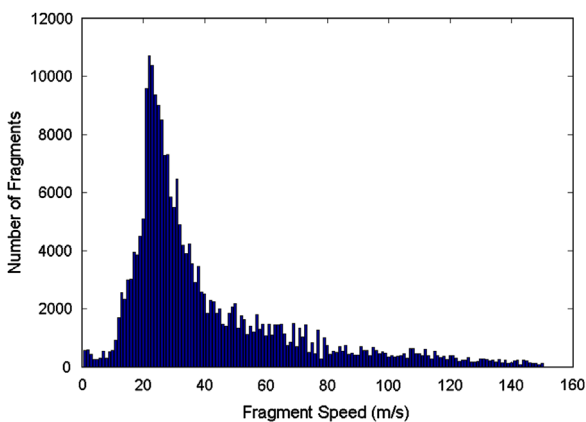


Fig. 5. Example of fragment velocity distribution.

the center of mass, as shown in Fig. 6. These are then integrated to predict an ephemeris for a 48-h period surrounding the nominal time of impact. Since coherent clouds of asteroid debris can reaggregate into a rubble pile for subcritical disruption energies [4,17,18], or

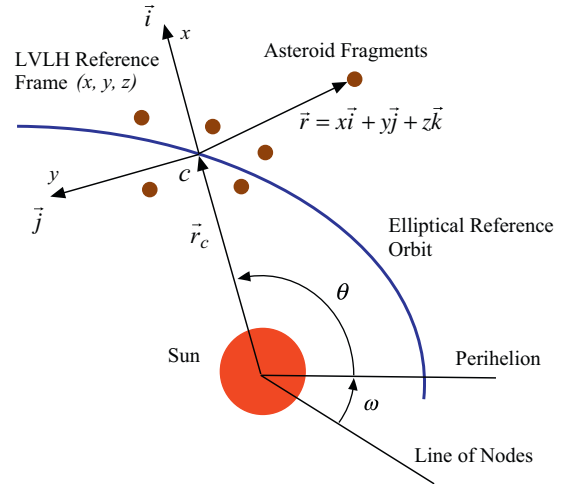


Fig. 6. LVLH reference frame.

remain a field of disruptive bodies [18,19], we implement a system for computing self-gravity among the resulting fragments. Since the LVLH reference frame is computationally beneficial for self-gravity and collision modelling among fragments [4], we use the non-linear relative equations of motion for this frame to govern fragment trajectories [4,8]:

$$\begin{aligned}\ddot{x}_i &= 2\dot{\theta} \left( \dot{y}_i - \frac{\dot{r}_c}{r_c} y_i \right) + \dot{\theta}^2 x_i + \frac{\mu}{r_c^2} - \frac{\mu}{r_d^3} (r_c + x_i) + \frac{\mu_E}{r_{Ei}^3} (x_E - x_i) + F_i^x \\ \ddot{y}_i &= -2\dot{\theta} \left( \dot{x}_i + \frac{\dot{r}_c}{r_c} x_i \right) + \dot{\theta}^2 y_i - \frac{\mu}{r_d^3} y_i + \frac{\mu_E}{r_{Ei}^3} (y_E - y_i) + F_i^y \\ \ddot{z}_i &= -\frac{\mu}{r_d^3} z_i + \frac{\mu_E}{r_{Ei}^3} (z_E - z_i) + F_i^z\end{aligned}\quad (7)$$

where  $x$ ,  $y$ ,  $z$ ,  $r_c$ , and  $\theta$  are defined as shown in Fig. 6,  $r_d$  is the length of the relative coordinate vector,  $\mu$  and  $\mu_E$  are gravitational parameters for the sun and the Earth,  $r_{Ei}$  is the distance from each fragment to Earth, and  $(F^x, F^y, F^z)$  are the combined acceleration components due to the 3rd body gravitational terms (solar system major body model [8]), self-gravity, and collision corrections. The threading structure for computing the values for self gravity terms is described in [4], while collisions are predicted using a Sort-and-Search algorithm [20], resulting in post-collision changes to position and velocity of fragments. An elastic spherical collision model is assumed for the fragments, with a coefficient of restitution of 0.5. For the fragments remaining on trajectories impacting Earth, we simulate reentry assuming solid granite material (a worst case) and a static (time independent) atmospheric density [8]. This gives a rough estimate on the amount of material ablated through atmospheric heating and the number of fragments that are deflected or disrupted by the atmosphere.

### 3.1. Timing and initial explosive energy

Fast computation of the resulting fragmented system allows for rapid parameter variation to determine optimal mission design parameters. Two quantities of significant interest are the amount of lead time between deflection

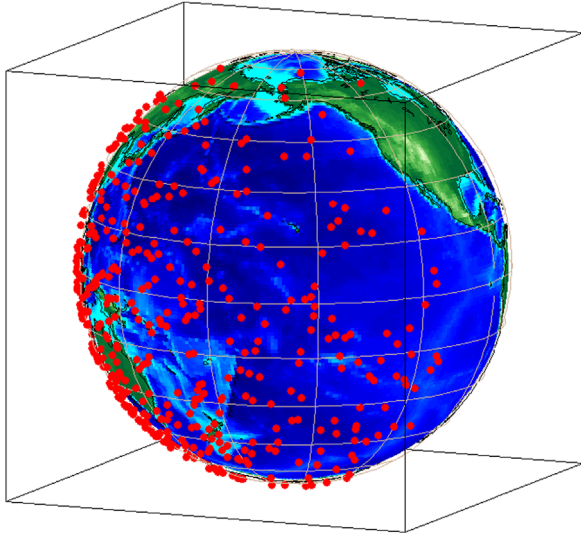


Fig. 7. Example of impact location distribution.

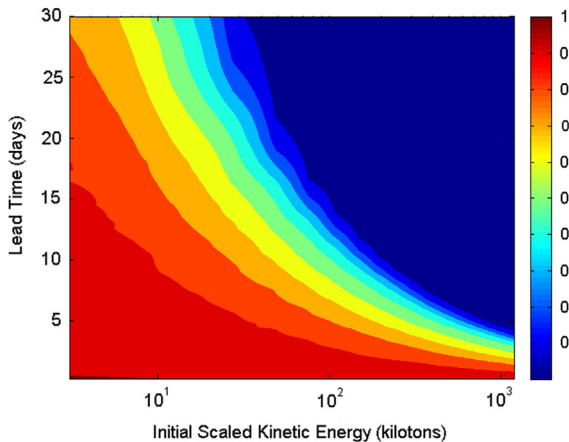


Fig. 8. Contour plot for impact mass parameter study.

and impact, and the amount of kinetic energy imparted to the fragments in the deflection event. It is believed that a nuclear payload is necessary to get the initial energy required to deflect the majority of a 270-m asteroid with up to one full orbit lead time (about 1000 days) [5]. An example of how impacting mass changes with timing and initial energy scaling can be seen in Fig. 8. These contours are colored by the fraction of original mass the impacts the Earth. Additionally, the benefit of additional lead time slows substantially above 30 days, revealing that 30 days might be a good target for mission design. For lead times below 10 days, an adequate deflection measure requires far more energy than generally available, suggesting the need for multiple deflection missions in this regime [5].

#### 4. Computational structure

This section addresses the computational approach used to solve the disruption problem. Each state variable update for a fragment is conducted in parallel at each

time step. A variety of hardware was available for this project, with a substantial difference in performance. This allowed us to get reasonable estimates on the computational cost of this simulation, in comparison to manufacturer performance numbers. Performance can vary based on the type of arrays used, and the number of threads dedicated to each GPU calculation. These factors are determined by the CUDA Compute Capability (CUDA CC), which is a property of the GPU [6]. These cost estimates are used to determine hardware performance on the various systems. A summary of the hardware used is shown in Table 3 (*Note*: all CPUs are Intel brand, and all GPUs are NVIDIA brand).

Each thread on the GPU calculates the state variable change for one fragment, with the GPU kernel limited to one time step. This is necessary because the positions of the planets and other gravitating bodies must be calculated and transferred to the GPU at each time step. Additionally, the positions of fragments at each integration substep are shared among multiple GPUs and CPU threads. For this reason, the present model is predominantly bandwidth-limited for small data sets. While grid information is not retained, one of the disadvantages of the SPH hydrocode is that neighboring particles must be calculated at each time step. Our approach in this model is to create a bounding volume for each SPH particle and perform the same Sort and Sweep in parallel as used to detect collisions in the orbital model [20]. We retain the information for neighbors connected by material strength, as well as carrying neighbor information through the correction step of the integrator. This results in a 28% performance improvement over recalculating neighbors at both the prediction and correction steps, while allowing for a variable time step based on the Courant condition [9,10]:

$$\delta t = \min_i \frac{h_i}{c_i} \quad (8)$$

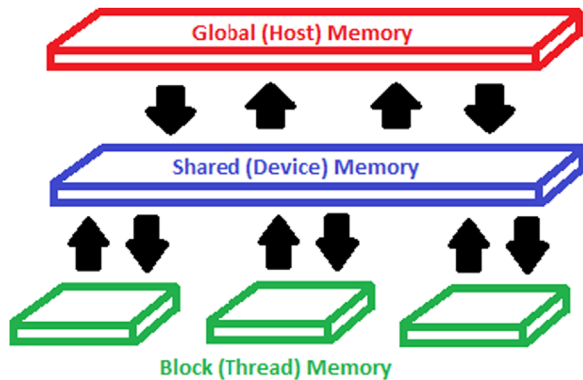
where  $c$  is the local sound speed. While the reduction operation to determine the new time step can be done in parallel, all GPU threads must have position information for all particles to determine neighbors. This requirement could be eliminated through clever domain decomposition, but there is a tradeoff between associating a mesh to the model and taking advantage of contiguous memory sections of particles. Load balancing would also require additional communication between GPUs, which has an impact on performance, as PCI-E bandwidth is one of the limiting factors in GPU acceleration [6].

Our memory model for this simulation includes a shared host memory, distributed device memory for each GPU, and data transfers between them handled through explicit array transfer. Each block of compute threads on the GPU takes the data it needs from the global device memory when the kernel reaches its block. This is an important factor, because the varying compute capabilities have different limitations on this block memory, changing the number of threads that may be used in the calculation. Constants are transferred to all GPU memories implicitly using a pointer to the host constant value. Fig. 9 shows an overview of this computational memory model.

**Table 3**

Hardware description for benchmark systems.

| System    | Machine 1       | Machine 2      | Machine 3       | Machine 4       |
|-----------|-----------------|----------------|-----------------|-----------------|
| CPU       | 1 × Core2 Q6600 | 1 × Xeon X5550 | 2 × Xeon E5520  | 2 × Xeon X5650  |
| CPU cores | 4               | 4              | 8               | 12              |
| CPU TPEAK | 9.6 GFLOPs      | 12.8 GFLOPs    | 21.36 GFLOPs    | 32.04 GFLOPs    |
| GPU       | 1 × GTX470      | 1 × GTX480     | 4 × Tesla c1060 | 4 × Tesla c2050 |
| GPU cores | 448             | 480            | 960             | 1792            |
| GPU TPEAK | 324 GFLOPs      | 385 GFLOPs     | 336 GFLOPs      | 2060 GFLOPs     |
| CUDA CC   | CC 2.0          | CC 2.0         | CC 1.3          | CC 2.0          |

**Fig. 9.** Qualitative computational memory model.

While modern dedicated compute GPUs have a high amount of onboard memory, it usually is far less than system memory. Though it may seem advantageous to calculate parameters for every time step before the start of the simulation, the arrays resulting from this approach are quite large. Each model of GPU has a limited number of memory registers available to each computing block of threads [6]. Therefore, the use of several large arrays can actually slow down the simulation in some cases, by lowering the number of threads below the maximum allowed by the architecture. This trades off directly with the added expense of calculating parameters on the Host at each time step. For the present work, calculating planetary positions and other simulation parameters at each step was found to be preferable to using a large pre-calculated array. For some hardware, sufficient GPU memory was not available for the latter method, so a heterogeneous computing approach proved to be the most portable.

## 5. Results

The initial stages of the impactor can be seen in Fig. 3. This is colored according to material state in the computer code and is captured immediately after the explosive energy release in the inner part of the penetrator. The resulting hot gas of explosive remnants disperses the rubble and fractures the core down to the representative particle size. While fragment size prediction was not available for this work, the current SPH approach would be one of a handful of approaches for investigating representative fragment sizes, since most grid-based

models would have to be interpolated, such as the ALE code used in [7]. An example of the increase in density for the 54 m target, with an expansion region behind the shock creating a jet of hot gas, can be seen in Fig. 4. The resulting mass-averaged fragment velocities are on the order of 10–100 m/s, similar to that for a static subsurface explosion [7], with a definite direction of the highest momentum in the direction of the penetrator motion. An example distribution of these velocities is shown in Fig. 5. This simulation framework is equally valid for oblique impacts, and should allow for direct implementation in conjunction with deflection mission planning.

The mass left on impacting trajectories is around 0.1% for a radial (outward) deflection with 15 days between the deflection attempt and the impact date. This target window is extremely beneficial from an engineering standpoint, as there is strong coupling between time-to-impact and a reduction in mission fuel cost [21]. High energy methods such as nuclear explosives are the only known way to produce results on such a short time frame. The present work shows that a well-designed impactor mission can achieve similar results with a contact burst as were previously predicted for a subsurface explosion. The benefit to the former method is that it does not require a rendezvous, and therefore there are available launch windows for this orbit over the entire period from 2029 to 2036 [21].

The reentry modeling has been shown to reduce the amount of impacting mass by about 90% [8]. While the remaining fragments could cause significant harm in populated areas, or through tsunami events, the impacts are below the threshold for an extinction event. This may indicate that nuclear disruption would be a desired outcome for a late-notice or late-decision scenario. Geocentric coordinates of these impacting events are calculated in order to provide a description of distance between impacts in both space and time. An example of this is shown in Fig. 7.

As shown in Fig. 10, the impacting mass for a fragmented system with 15-day lead time can be very low, even including self-gravity and collisions among the fragments that dissipate energy. The present SPH hydrocode suggests that a dynamic model of a hypervelocity surface burst yields results similar in spatial and temporal distribution to a static subsurface explosion. This gives additional launch windows for mission design, limits the fuel needed for a rendezvous burn, and avoids the need to bury the explosive payload. Additionally, the dynamic model should better predict system behavior when addressing high velocity penetrator architectures.

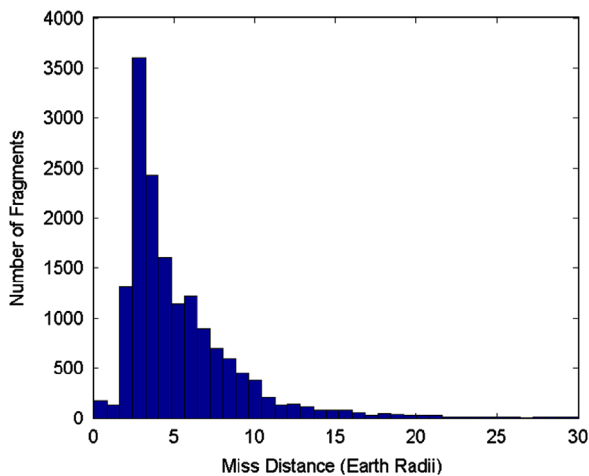


Fig. 10. Miss distance histogram for 15-day lead time.

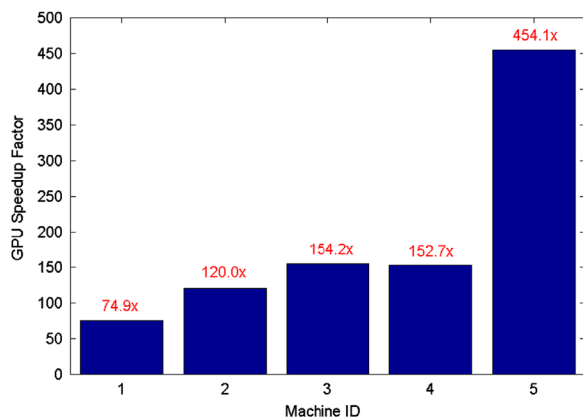


Fig. 11. GPU speedups for 54-m target asteroid model.

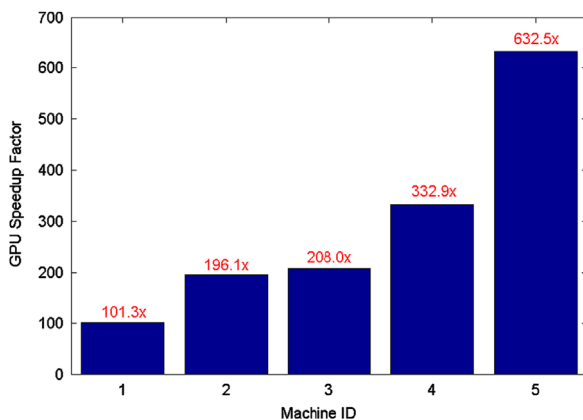


Fig. 12. GPU speedups for 270-m target asteroid model.

This might give an option for realistically determining the limits of such a system for asteroid deflection missions.

New HPC technology utilizing GPU acceleration have resulted in orders of magnitude improvement in computational ability. Figs. 11 and 12 show speedup of the GPU accelerated model compared to serial execution for the

54-m and 270-m target models. While the 233,000 particles of the 54-m target are limited mostly by communication bandwidth, the 1.4 million particles in the 270-m model are limited by computational speed and memory bandwidth for the threads on the GPU. A substantial speedup improvement, from  $454\times$  to  $632\times$ , is observed. This shows single node computational performance on the same order as a moderate cluster. The ability to run multiple cases to address statistical system behavior results in simulation being integrated into overall mission design. Mission effectiveness can be estimated in advance of a need for mission design, allowing new architectures and interchangeable components for a universal deflection plan.

## 6. Conclusion

This paper outlined the development of software and hardware tools to aid the planning of NEO deflection mission design, and the current project strives to identify key technologies for effective implementation. While the assumed target structure is so simple as to be non-physical, it is possibly representative of the fragmentation results that could be applied to a variety of bodies. Disruption of a Hazardous NEO on an impacting trajectory is a feasible solution with short warning time, provided some impacting mass is assumed inevitable. Improved simulation capabilities allow us to better quantify the material composition characteristics that will most affect our ability to mitigate a threat. We now have the technology and resources to move from threat to action, and a new era of planetary defense where we can focus on developing a standing threat mitigation capability is on the horizon.

## References

- [1] M. Boslough, Airburst warning and response, in: Proceedings of the IAA-PDC-2166721, 2nd IAA Planetary Defense Conference, Bucharest, Romania, May 9–12, 2011.
- [2] Committee to Review Near-Earth Object Surveys and Hazard Mitigation Strategies, in: Defending Planet Earth: Near-Earth Object Surveys and Hazard Mitigation Strategies, National Research Council, 2010.
- [3] J. Sanchez, M. Vasile, G. Radice, On the consequences of a fragmentation due to a NEO mitigation strategy, in: Proceedings of the IAC-08-C1.3.10, 59th International Astronautical Congress, Glasgow, United Kingdom, September 29 – October 3, 2008.
- [4] B. Kaplinger, B. Wie, Optimized GPU simulation of a disrupted near-Earth object including self-gravity, in: AAS-11-266, 21st AAS/AIAA Spaceflight Mechanics Meeting, New Orleans, LA, February 13–17, 2011.
- [5] B. Kaplinger, B. Wie, Parameter variation in near-Earth object disruption simulations using GPU acceleration, in: AAS-11-267, 21st AAS/AIAA Spaceflight Mechanics Meeting, New Orleans, LA, February 13–17, 2011.
- [6] D.B. Kirk, W.W. Hwu, Programming Massively Parallel Processors, Morgan Kaufmann, Burlington, 2010.
- [7] B. Wie, D. Dearborn, Earth impact modeling and analysis of a near-Earth object fragmented and dispersed by nuclear subsurface explosions, in: AAS-10-137, 20th AAS/AIAA Spaceflight Mechanics Meeting, San Diego, CA, February 14–17, 2010.
- [8] B. Kaplinger, B. Wie, D. Dearborn, Preliminary results for high-fidelity modeling and simulation of orbital dispersion of asteroids disrupted by nuclear explosives, in: AIAA-2010-7982, AIAA/AAS Astrodynamics Specialist Conference, Toronto, Ontario, Canada, August 2–5, 2010.

- [9] J.J. Monaghan, Smoothed particle hydrodynamics, Rep. Prog. Phys. 68 (July) (2005) 1703–1759.
- [10] G.R. Liu, M.B. Liu, Smoothed Particle Hydrodynamics: A Meshfree Particle Method, World Scientific Publishing, Singapore, 2003.
- [11] W. Benz, E. Asphaug, Simulations of brittle solids using smooth particle hydrodynamics, Comput. Phys. Commun. 87 (1995) 253–265.
- [12] S. Hiermaier, D. Konke, A.J. Stimp, K. Thoma, Computational simulation of the hypervelocity impact of al-spheres on thin plates of different materials, Int. J. Impact Eng. 20 (1997) 363–374.
- [13] M. Jutzi, W. Benz, P. Michel, Numerical simulations of impacts involving porous bodies I. Implementing sub-resolution porosity in a 3D SPH hydrocode, Icarus 198 (2008) 242–255.
- [14] P.W. Randles, L.D. Libersky, Smoothed particle hydrodynamics: some recent improvements and applications, Comput. Methods Appl. Mech. Eng. 139 (1996) 375–408.
- [15] J.H. Tillotson, Metallic Equations of State for Hypervelocity Impact, General Atomic Technical Report GA-3216, 1962.
- [16] S.H. Schuster, J. Isenberg, Equations of State for Geologic Materials, Defense Nuclear Agency Technical Report DNA-2925Z, 1972.
- [17] S.G. Love, T.J. Ahrens, Catastrophic impacts on gravity dominated asteroids, Icarus 124 (1996) 141–155.
- [18] E. Asphaug, S.J. Ostro, R.S. Hudson, D.J. Scheeres, W. Benz, Disruption of kilometre sized asteroids by energetic collisions, Nature 393 (1998) 437–440.
- [19] P. Michel, W. Benz, D.C. Richardson, Disruption of fragmented parent bodies as the origin of asteroid families, Nature 421 (February) (2003) 608–611.
- [20] S. LeGrand, Broad-phase collision detection with CUDA, in: H. Nguyen (Ed.), GPU Gems 3, Addison-Wesley, 2007.
- [21] S. Wagner, B. Wie, Analysis and design of fictive post-2029 apophis intercept mission for nuclear disruption, in: AIAA-2010-8375, AIAA/AAS Astrodynamics Specialist Conference, Toronto, Ontario, Canada, August 2–5, 2010.